Int. J. Radiation Oncology Biol. Phys., Vol. 82, No. 5, pp. 1903–1911, 2012

0360-3016/$ - see front matter

ELSEVIER

doi:10.1016/j.ijrobp.2011.01.040

CLINICAL INVESTIGATION **Genitourinary Cancer**

PRACTICAL METHOD OF ADAPTIVE RADIOTHERAPY FOR PROSTATE CANCER USING REAL-TIME ELECTROMAGNETIC TRACKING

JEFFREY R. OLSEN, M.D., CAMILLE E. NOEL, B.S., KENNETH BAKER, C.M.D., LAKSHMI SANTANAM, PH.D., JEFF M. MICHALSKI, M.D., AND PARAG J. PARIKH, M.D.

Department of Radiation Oncology, Washington University School of Medicine, St. Louis, MO

Purpose: We have created an automated process using real-time tracking data to evaluate the adequacy of planning target volume (PTV) margins in prostate cancer, allowing a process of adaptive radiotherapy with minimal physician workload. We present an analysis of PTV adequacy and a proposed adaptive process.

Methods and Materials: Tracking data were analyzed for 15 patients who underwent step-and-shoot multi-leaf collimation (SMLC) intensity-modulated radiation therapy (IMRT) with uniform 5-mm PTV margins for prostate cancer using the Calypso® Localization System. Additional plans were generated with 0- and 3-mm margins. A custom software application using the planned dose distribution and structure location from computed tomography (CT) simulation was developed to evaluate the dosimetric impact to the target due to motion. The dose delivered to the prostate was calculated for the initial three, five, and 10 fractions, and for the entire treatment. Treatment was accepted as adequate if the minimum delivered prostate dose (D_{min}) was at least 98% of the planned D_{min}.

Results: For 0-, 3-, and 5-mm PTV margins, adequate treatment was obtained in 3 of 15, 12 of 15, and 15 of 15 patients, and the delivered D_{min} ranged from 78% to 99%, 96% to 100%, and 99% to 100% of the planned D_{min}. Changes in D_{min} did not correlate with magnitude of prostate motion. Treatment adequacy during the first 10 fractions predicted sufficient dose delivery for the entire treatment for all patients and margins.

Conclusions: Our adaptive process successfully used real-time tracking data to predict the need for PTV modifications, without the added burden of physician contouring and image analysis. Our methods are applicable to other uses of real-time tracking, including hypofractionated treatment. © 2012 Elsevier Inc.

Prostate, Cancer, Radiotherapy, Intrafraction, Adaptive.

INTRODUCTION

Multiple randomized clinical trials have demonstrated a dose escalation benefit for prostate radiotherapy (1–5). Recent data suggest that both inter- and intrafraction prostate motion are not negligible (6–11). Selection of planning target volume (PTV) margins must balance ensurance of adequate dose delivery to the prostate with the hazard of increased dose to normal tissues (12).

Given the heterogeneity of intrafraction motion among patients previously described (10, 11, 13), patients with minimal intrafraction motion may benefit from PTV margin reductions. Although numerous methods are available to quantify isolated translational prostate motion, the dosimetric consequences of translational and rotational motion are not well described. Current methods of dose verification rely on serial imaging and contouring, which create a segmentation and image analysis workload for the physician. These methods cannot account for all intrafraction motion, as images are not sampled continuously throughout treatment.

We have created an automated process using real-time electromagnetic tracking to evaluate adequacy of PTV margins in prostate cancer, allowing a practical method of adaptive radiation therapy with reduced physician workload.

The purposes of this study were (*1*) to determine whether patient-specific rotations and translations of the prostate could predict adequacy of plans with 0-, 3-, and 5-mm margins, and (*2*) to determine whether rotations and translations from the first three, five, or 10 fractions could predict adequacy of the margins for the remainder of therapy.

METHODS AND MATERIALS

Patient population

Records were analyzed for 15 patients who underwent definitive intensity-modulated radiation therapy (IMRT) for prostate cancer

Reprint requests to : Parag J. Parikh, M.D., Department of Radiation Oncology, Washington University School of Medicine, 4921 Parkview Place, Lower Level, St. Louis, MO 63110. Tel: (314) 362-8525; Fax: (314) 362-8521; E-mail: pparikh@radonc.wustl.edu

Supported in part by National Cancer Institute Grant R01CA134541.

Conflict of interest: Research interface provided by Calypso Medical Technologies. Dr. Parikh receives research funding from Calypso Medical Technologies.

Acknowledgment—This research was first presented at the 51st annual meeting of the American Society for Radiation Oncology, November 1-5, 2009, in Chicago, IL.

Received Dec 14, 2009, and in revised form Jan 11, 2011. Accepted for publication Jan 26, 2011.

Table 1. Patient characteristics

No. of patients	15
Median age, y	71
Age range, y	58–83
Tumor stage	
T1c	12
T2a	1
T3a	1
T3b	1
Risk stratification	
Low	9
Medium	4
High	2
Median prescribed dose, Gy (range)	7,380 (7,000–7,920)

using the Calypso® 4D Localization System (Calypso Medical, Seattle, WA) between November 2007 and March 2009. Most patients had low-risk disease (14). Patient characteristics are shown in Table 1.

Simulation and treatment planning

Details of our methods for magnetic resonance imaging (MRI) simulation, subsequent transponder placement, and computed tomography (CT) simulation have been previously described (15). Planning CT and MR images were imported into Pinnacle v8.0m (Philips Medical Systems, Cleveland, OH) and fused with manual, rigid image registration using prostate anatomy contoured on both the CT and MRI scans. The clinical target volume (CTV) was formed by contouring the prostate on the CT and MR fusion images (Fig. 1).

For each patient, 0-mm, 3-mm, and 5-mm expansions were applied about the prostate to create PTV volumes. Five-field IMRT plans using a step-and-shoot multi-leaf collimation (SMLC) technique were generated with a planning goal of 100% CTV and 98% PTV coverage by prescription dose. Rectal constraints were applied such that the rectal volumes receiving greater than 65 Gy (V65) and 40 Gy (V40) were less than 17% and 35%, respectively. Bladder constraints were applied such that the volumes of bladder receiving dose greater than 65 Gy and 40 Gy were less than 25% and 50%, respectively. Figure 1 illustrates a representative plan for 1 patient treated with a 5-mm PTV margin.

Treatment delivery

Real-time electromagnetic tracking was used for all patients obtained at 0.1-s intervals. The Calypso system reports set-up rotations/translations and intrafraction prostate position. Therapists are alerted to displacements exceeding motion limits via feedback provided by the system's graphical display and audible alarms. Radiation delivery was initiated only if reported setup rotation was less than 10°. If setup rotation exceeded 10°, patients were repositioned and then, if necessary, asked to urinate to adjust bladder filling. Treatment was delivered only while isocenter deviation was less than 3 mm from setup during real-time tracking to prevent radiation delivery during large anatomical variations. An example motion trace of a treatment delivery pause followed by couch repositioning is shown in Fig. 2.

Motion analysis

Using a research feature of the Calypso system that allows for tracking data export, the three-dimensional spatial coordinates for each transponder were sampled at 0.1-s intervals during treatment.

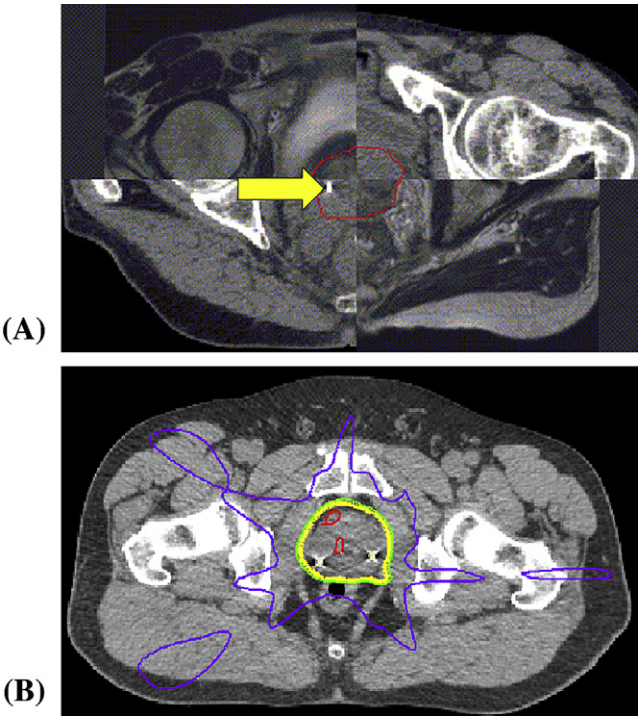

Fig. 1. (A) Checkerboard axial image of the fused magnetic resonance imaging (MRI) and computed tomography (CT) scans, and the contoured prostate, illustrated for 1 patient. The final contoured prostate (clinical target volume [CTV]) is shown in red. A fiducial beacon placed at the right base of the prostate is seen on this CT slice (arrow). (B) Isodose distribution of a 5-field intensity-modulated radiation therapy (IMRT) prostate plan, showing the 50% (purple), 95% (green), 100% (yellow), and 105% (red) isodose lines.

A custom Matlab program called SWIFTER (Semi-Automatic Workflow using Intra-fraction Fiducial-based Tracking for Evaluation of Radiotherapy) was used to estimate delivered dose using the static dose cloud from treatment planning along with the measured intrafraction motion. The details and validation of the software application have been previously described (16). Briefly, rotation was calculated about each axis (superior/inferior, anterior/posterior, right/left), with the origin set at the centroid of the three transponders. Using SWIFTER, target motion within the planned dose cloud was simulated using measured translations and rotations collected over each patient's course of therapy in order to gauge the "actual delivered dose" to the prostate. This analysis requires no physician input or recontouring, because the prostate structure is obtained from the planning CT and rigidly translated and rotated through the static dose cloud from the treatment plan. A simulation of the prostate structure moving relative to the dose cloud for a sample translation/rotation is shown in Fig. 3. For each patient, the dose delivered to the prostate was calculated for the first three, five, and 10 fractions, and for the entire treatment.

Evaluation of rigid body approximation

To assess the validity of this approximation in our cohort, intertransponder distances (sampled at 0.1-s intervals throughout treatment) were analyzed for variation. Histogram plots of the distribution of tracked intertransponder distances compared with the mean for each patient were generated. To evaluate deformation,

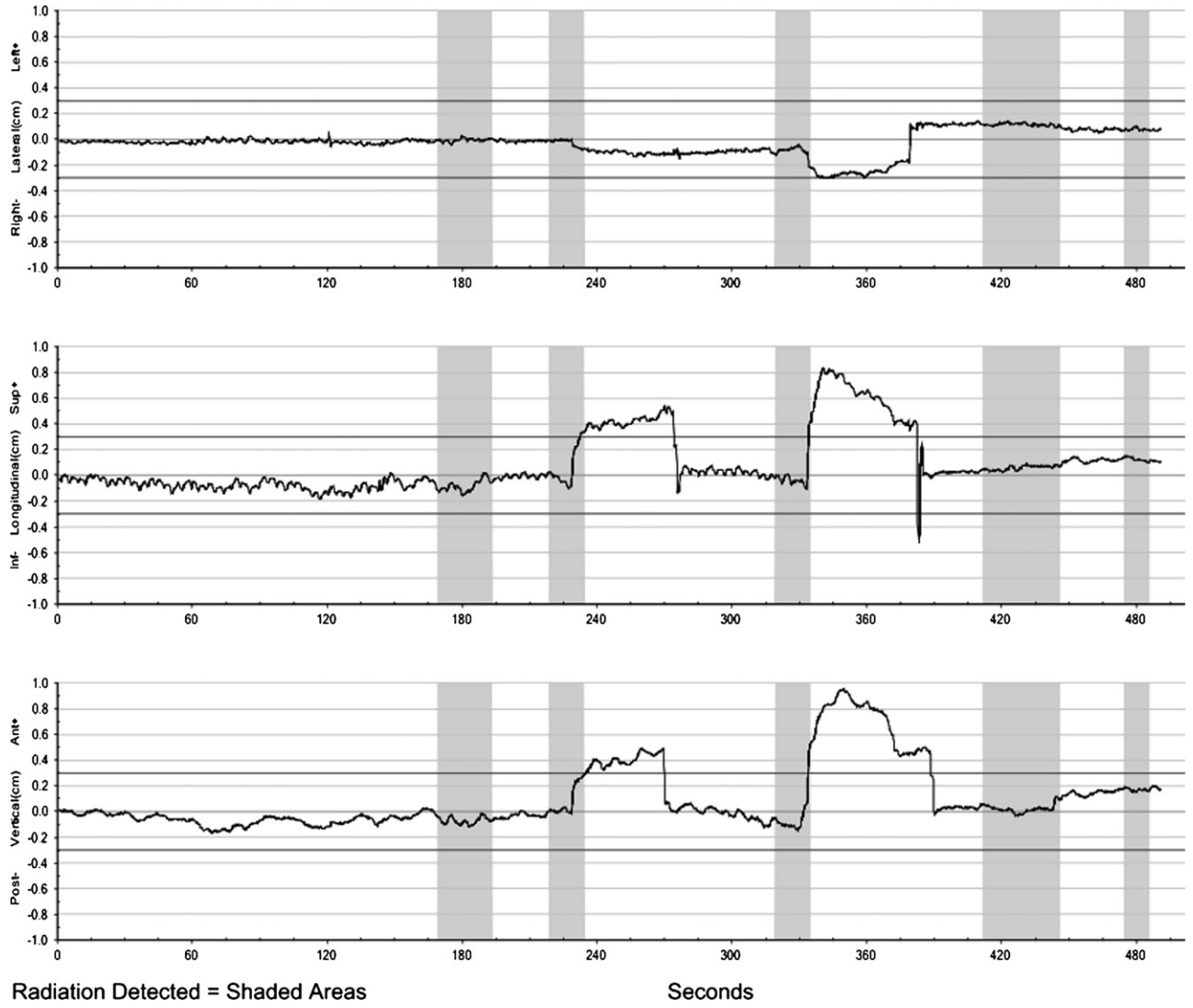

Fig. 2. Real-time tracking data for one treated fraction, including, including right–left (top), superior–inferior (middle), and anterior–posterior (bottom) tracking data. Shaded regions illustrate the time when the treatment beam was turned on for each of the five planned fields. After delivery of the second field, treatment was paused because of a persistent shift in the superior and anterior directions that exceeded tolerance. This was corrected with intrafraction repositioning 270 s into treatment. Additional repositioning was used at 380 s after delivery of the third field because of motion in the right, superior, and anterior directions that exceeded tolerance.

variability of the measured intertransponder distances was compared with the known positional accuracy of the tracking system (<0.5 mm) (17).

Evaluation of variable rectal anatomy

Day-to-day changes in rectal composition could potentially modify the radiation dose distribution, particularly at the rectum–prostate interface. Because the dose distribution was modeled as unchanging, interfraction change in dose cloud shape could potentially introduce a calculation error. To evaluate our static dose cloud approximation, we studied the effect of a "worst-case" change in rectal composition by manual assignment of air-equivalent density (0 g/cc) to the rectum for 1 patient with rectal distension at simulation. Aside from rectal tissue density, all parameters for the IMRT plan were kept constant. To evaluate dose at the rectum–prostate interface, a new structure (RP Interface) was created by expanding the prostate 1 mm posteriorly, followed by subtraction of the initial prostate structure. Maximum, minimum, and mean doses to the prostate and RP Interface were calculated for comparison between the standard and worst-case plans. The percent volume of prostate receiving 95% prescription dose was also calculated, and isodose lines for 95% and 50% of prescription dose were also compared.

Evaluation of PTV adequacy

PTV adequacy was assessed using dose statistics of the prostate structure. The "actual" minimum dose delivered to the prostate (D_{min}) based on our simulation was calculated both for the first three, five, and 10 treatments, and for the entire treatment course. In addition, dose delivered to 95% of the prostate volume (D95) was calculated for the entire course. In accordance with our planning constraints, adequate treatment was defined as a course in which the actual delivered dose to the prostate was no less than 98% of the planned minimum dose.

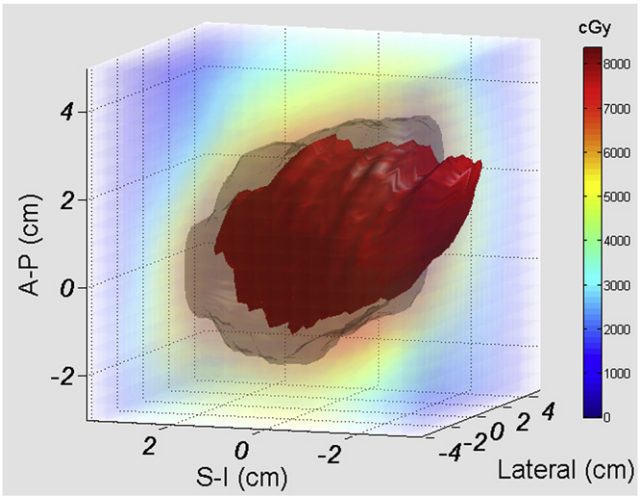

Fig. 3. Illustration of the impact of translational and rotational motion for a prostate (red) plan using a 3-mm planning target volume (PTV) margin (gray), with prostate rotation of 20° pitch, and translational shifts of 3 mm in the anterior and inferior directions. Real-time tracking translational and rotational data were used to virtually move the prostate within the treatment dose cloud, to estimate the "actual" dose delivered for each patient's motion.

Correlation of patient motion parameters with treatment adequacy

Pitch, roll, and yaw rotation, and isocenter translational displacement along each axis (superior–inferior, anterior–posterior, right–left) and in total were tested for correlation with the decrement in delivered prostate dose to determine whether patient motion parameters could predict adequacy of treatment. Total displacement was defined as mean three-dimensional isocenter displacement over an entire treatment course from the planned position as defined by the distance formula. Scatter plots and linear regression were performed to determine whether specific rotations and translations predict inadequate D_{min} as measured by SWIFTER.

Treatment adequacy prediction using analysis of initial treatments

We evaluated whether dose coverage during the first few radiotherapy fractions predicted adequacy for an entire treatment course, and also determined the number of fractions required to successfully predict treatment adequacy. Delivered D_{min} values as a percentage of planned D_{min} were calculated using the tracking data from the first three, five, and 10 fractions. Coverage adequacy based on D_{min} during each initial treatment period was compared with the D_{min} for each patient's entire treatment course. D_{min} was calculated as the cumulative delivered dose using all available data at a given time point, rather than for each fraction individually.

Impact of translational and rotational motion on rectal dose

To assess the impact of translational and rotational motion on rectal dose, contours were generated to contain the portion of the rectum lying within 2 cm of the prostate contour. The 2-cm cut-point was arbitrarily chosen because of concern regarding the applicability of a rigid body transformation if the entire rectum contour were used. Using SWIFTER, "actual" rectal doses were calculated using each patient's real-time tracking data, and comparisons were made with the planned rectal doses (V40 and V65), both for the 3-mm and 5-mm PTV plans.

RESULTS

Treatment plans

Treatment plan parameter results are illustrated in Table 2. No significant planning differences were observed in PTV coverage for the 0-mm, 3-mm, and 5-mm margin plans (p = NS, Student's paired two-tailed t-test) as gauged by the percentage of the prescription dose delivered to 98% of each PTV. Statistically significant decrements (Table 2) were noted in the volumes of rectum and bladder receiving 65 Gy and 40 Gy as PTV margins were reduced from 5 mm to 3 mm and from 3 mm to 0 mm (Student's paired two-tailed t-test; Table 2).

Translational and rotational motion

Across all patients, compared with position at the time of simulation, the mean and standard deviation values of the magnitude of rotation about the x (pitch), y (roll), and z (yaw) axes were 5.7° ± 5°, 2.0° ± 2°, and 1.6° ± 1°. The mean and standard deviation of the magnitude of translation in the x (anterior–posterior), y (left–right), and z (superior–inferior) directions were 0.39 mm ± 0.4 mm, 0.64 mm ± 0.5 mm, and 0.69 ± 0.6 mm. Table 3 illustrates the mean rotation about the x, y, and z axes, as well as the mean translational displacement along each axis and in total for each patient. Substantial variation in the magnitude of patient motion was seen across the study's population (Table 3).

Evaluation of rigid body approximation

Figure 4 displays the histogram of intertransponder distances for all patients across all fractions. Intertransponder

Table 2. Impact of planning target volume (PTV) margins on doses delivered to rectum and bladder

PTV margin	% Rx dose delivered to 98% of PTV	Rectum V65	Rectum V40	Bladder V65	Bladder V40
0 mm	100.6 ± 0.7	3.5 ± 3	14.6 ± 6	4.3 ± 5	16 ± 10
3 mm	100.7 ± 0.7	7.5 ± 4	19.8 ± 6	9 ± 10	22 ± 20
5 mm	100.5 ± 2	10.0 ± 4	23.3 ± 7	12 ± 10	26 ± 20
p Value (0 mm, 3 mm)	0.6	<0.001	<0.001	0.003	<0.001
p Value (3 mm, 5 mm)	0.7	<0.001	0.005	0.001	<0.001

Abbreviations: Rx = prescription/prescribed; V65 = percentage of organ receiving ≥65 Gy. V40 = percentage of organ receiving ≥40 Gy. A significant reduction in rectal and bladder V65 and V40 values was seen for reductions in PTV margins.

Table 3. Characteristics of each patient's rotational and translational motion

	Mean magnitude of rotation (°)			Mean isocenter displacement (mm)			
Patient no.	x–Axis (pitch)	y-Axis (roll)	z-Axis (yaw)	Sup–Inf	Ant–Post	Left–Right	Composite
1	3.1 ± 3	0.71 ± 0.7	0.31 ± 0.5	0.48 ± 0.4	0.51 ± 0.5	0.71 ± 0.6	1.18 ± 0.6
2	4.3 ± 3	2.3 ± 1	4.5 ± 1	0.58 ± 0.5	0.68 ± 0.5	0.37 ± 0.3	1.11 ± 0.5
3	5.9 ± 3	3.4 ± 1	1.6 ± 0.9	0.46 ± 0.4	0.76 ± 0.7	0.30 ± 0.4	1.13 ± 0.5
4	12.5 ± 4	1.9 ± 1	2.38 ± 0.9	0.74 ± 0.5	0.51 ± 0.4	0.35 ± 0.4	1.14 ± 0.5
5	4.0 ± 3	2.9 ± 2	2.18 ± 0.8	0.60 ± 0.5	0.60 ± 0.6	0.40 ± 0.4	1.10 ± 0.7
6	5.3 ± 2	1.33 ± 0.9	1.84 ± 0.9	0.46 ± 0.4	0.62 ± 0.6	0.29 ± 0.3	0.99 ± 0.6
7	3.8 ± 3	2.6 ± 2	2.5 ± 1	0.68 ± 0.6	0.42 ± 0.5	0.57 ± 0.5	1.13 ± 0.6
8	12.0 ± 5	1.3 ± 1	1.40 ± 0.9	0.77 ± 0.6	0.89 ± 0.7	0.34 ± 0.4	1.43 ± 0.7
9	2.4 ± 2	1.4 ± 1	0.74 ± 0.6	0.57 ± 0.5	0.90 ± 0.7	0.43 ± 0.4	1.34 ± 0.6
10	5.2 ± 4	2.5 ± 2	0.90 ± 0.8	0.70 ± 0.5	0.84 ± 0.7	0.42 ± 0.4	1.40 ± 0.7
11	4.4 ± 3	2.2 ± 2	1.5 ± 1	0.83 ± 0.7	0.85 ± 0.7	0.39 ± 0.4	1.43 ± 0.8
12	3.7 ± 2	2.7 ± 1	0.70 ± 0.7	0.72 ± 0.6	0.74 ± 0.7	0.37 ± 0.3	1.27 ± 0.7
13	1.9 ± 2	1.14 ± 0.9	0.63 ± 0.6	0.64 ± 0.5	0.58 ± 0.5	0.49 ± 0.4	1.16 ± 0.5
14	6.4 ± 2	1.26 ± 0.9	3.1 ± 1	0.49 ± 0.5	0.56 ± 0.6	0.52 ± 0.4	1.08 ± 0.5
15	2.5 ± 2	1.18 ± 0.9	1.39 ± 0.8	0.63 ± 0.5	0.72 ± 0.6	0.21 ± 0.3	1.13 ± 0.6

Abbreviations: Ant = anterior; Inf = inferior; Post = posterior; Sup = superior.

distances varied by less than 0.5, 1, 1.5, and 2 mm from the average for 55%, 84%, 95%, and 99% of total treatment time, respectively. Given the known positional accuracy of 0.5 mm (17), intertransponder deformations greater than 0.5 and 1.5 mm occurred less than 16% and 1% of the total treatment time, respectively.

Evaluation of variable rectal anatomy

Figure 5 shows a sagittal image of the rectal contour with 95% and 50% isodose lines for actual tissue density and overridden (air-equivalent) tissue density, respectively. A slight but perceptible increase in the volume receiving 95% prescription is noted for the air-equivalent density calculation. The prostate minimum, maximum, and mean doses as a percentage of prescription were 100.7%, 107.3%, and 104.5% for the normal tissue density calculation and were 95.3%, 108.0%, and 104.7% for the air-equivalent density calculation. The RP interface, minimum, maximum, and mean doses as a percentage of prescription were 102.0%, 107.2%, and 104.8% for the actual tissue density calculation and were 93.4%, 107.3%, and 103.8% for the air-equivalent density calculation. Of the prostate, 100% received 95% prescription dose for both air and tissue density rectal calculations. A dose decrement anterior to the rectum was noted for the air-equivalent density calculation because of loss of lateral scatter at the air–tissue interface.

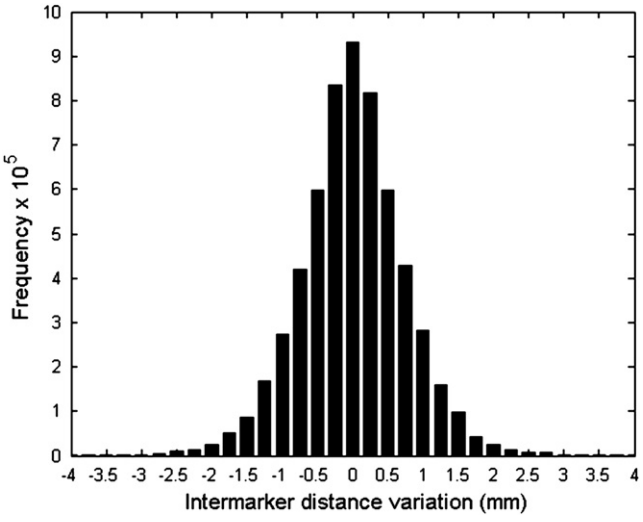

Fig. 4. Histogram of the intrafraction intertransponder distance variation from mean distance (mm) observed throughout treatment for all patients and fractions.

Dose effect of prostate motion

For 0-, 3-, and 5-mm PTV margins, adequate treatment was obtained in 3 of 15, 12 of 15, and 15 of 15 patients, and the delivered D_{min} ranged from 78% to 99%, 96% to 100%, and 99% to 100% of the planned D_{min}, respectively. In Table 4, the actual delivered prostate D_{min} is shown for each of the 15 patients and each PTV expansion as a percentage of the planned D_{min}. Delivered dose is shown both for the first 10 fractions and for the entire radiotherapy course of each patient. The D95 (minimum dose covering 95% of the prostate) was not affected by motion for any of the PTV margins. Delivered D95 remained within 1% and 2% of planned D95 for 44 of 45 and 45 of 45 cases. Figure 6 shows example "actual" and planned prostate and rectum (within 2 cm of the prostate) DVH curves for 2 patients (Patients 4 and 6).

Correlation of prostate motion with treatment adequacy

Figure 7 shows the dose decrement (change in actual vs. planned minimum prostate dose) as a function of mean pitch, roll, yaw, and displacement along each x (left–right), y (superior–inferior), and z (anterior–posterior) direction for all patients, using a 0-mm PTV expansion. No correlation was noted between dose decrement and mean pitch, roll, yaw, or any component of translational motion for any of the PTV expansions.

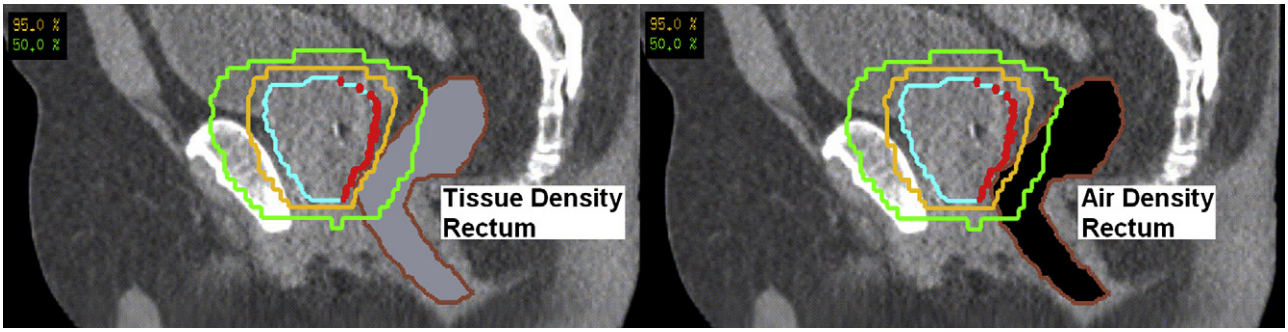

Fig. 5. Sagittal image showing 95% (orange) and 50% (green) isodose lines for a patient planned using a tissue density (left) compared to air-equivalent density (right) rectum structure. The rectum–prostate interface structure is shown in red.

Prediction of treatment adequacy based on initial treatments

For 30 cases of adequate treatment, motion analysis using only the first 3, 5, and 10 fractions predicted adequacy of the entire radiotherapy course in 26 of 30, 28 of 30, and 30 of 30 cases. For 15 cases of inadequate treatment, analysis using only the first three, five, and 10 fractions predicted inadequacy in 13 of 15, 14 of 15, and 15 of 15 cases, revealing a need for PTV expansion. Table 4 shows delivered dose to the prostate as a percentage of planned minimum dose for each PTV margin, based on the first 10 fractions and the entire treatment course for each patient.

Impact of translational and rotational motion on rectal dose

The volumes of rectum within 2 cm of the prostate and receiving greater than 40 Gy (V40) or greater than 65 Gy (V65) were not uniformly affected by prostate translational and rotational motion (Student's paired two-tailed *t*-test, $p = 0.8$ and 0.6 for 3-mm and 5-mm comparison of V40, and $p = 0.6$ and 0.9 for 3-mm and 5-mm comparison of V65), although some patient-specific variability was observed (Fig. 6).

Table 4. Minimum dose delivered to the prostate as a percentage of planned minimum dose for 0-, 3-, and 5-mm planning target volume (PTV) margins, based on the first 10 fractions and the entire treatment course of each patient

Patient no.	Minimum dose delivered to prostate as % of planned minimum dose (Goal >98%)					
	0–mm PTV		3–mm PTV		5–mm PTV	
	10 fx	All	10 fx	All	10 fx	All
1	99	99	100	100	100	100
2	94	93	99	99	100	100
3	89	89	96	96	99	99
4	89	89	96	96	100	99
5	92	97	99	100	99	100
6	86	78	100	99	100	100
7	96	97	100	100	100	100
8	90	88	99	100	101	101
9	94	97	100	100	101	100
10	95	93	101	101	100	100
11	92	96	98	99	101	101
12	92	92	100	100	100	100
13	98	99	100	100	100	100
14	88	87	97	97	100	100
15	98	99	100	100	100	100

Abbreviation: fx = fractions.

DISCUSSION

Our data confirm variation in intrafraction motion among patients that has been previously described (10, 11, 13) and provides the first analysis of the dosimetric implications of intrafraction motion, taking into account both translation and rotation. Li *et al.* (18) studied intrafraction translational motion using tracking data from 35 patients, applied to IMRT plans from 2 patients, and found that a 2-mm margin was sufficient. In our analysis, we accounted for both translational and rotational motion, and used each patient's treatment plan for the dose calculation, which showed the need for a larger margin in some patients.

Prior analyses of rotational motion have not accounted for individual patient anatomy. A previously published dosimetric study (19) suggested that prostate rotations greater than 5° may reduce 98% PTV coverage. For patients in our study (Patients 3, 4, and 14) for whom 3-mm plans were insufficient, mean pitch rotation was greater than 5°. However, such a degree of rotational motion did not always correlate with a decrement in dose delivered to the prostate.

We attempted to determine a correlation between specific motion factors (pitch, roll, yaw, displacement) and decrement in dose delivered. Interestingly, we were unable to determine any generalized motion parameters that would predict a decrement in delivered prostate dose. Figure 7 shows the poor correlation between the degree of prostate rotation/translation and dose decrement. The weakness of a generalized rotation threshold is shown by different effects of implant geometry, illustrated in Fig. 8. Rotations may take on increased or decreased significance because of a "lever arm" effect if the axis of measurement is at the periphery of the organ of interest. This effect likely contributes to the poor correlation between measured patient motion factors and dose decrement.

Our clinic uses D_{min} as a metric to define treatment adequacy, and we propose D_{min} as the most applicable parameter for prostate motion analysis because of the small prostatic

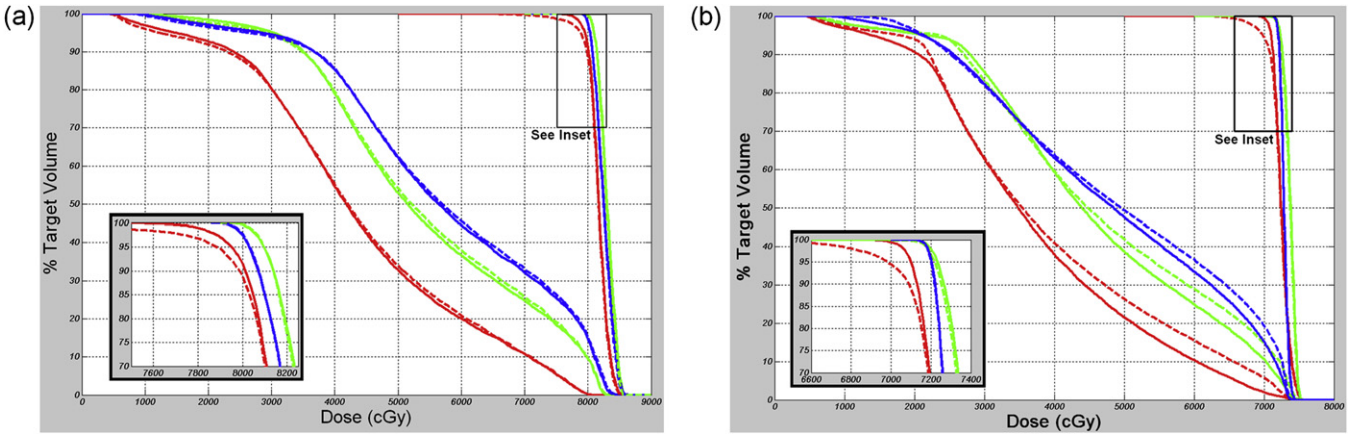

Fig. 6. Dose–volume histogram (DVH) curves for Patient 4 (a) and Patient 6 (b), illustrating "actual" (dotted) and planned (solid) dose for the clinical target volume (CTV; inset) and rectum, for 0-mm (red), 3-mm (green), and 5-mm (blue) planning target volume (PTV) margins.

volumes affected. The absence of a significant change in D95 for any patient confirms that dose alterations were seen in only a relatively small volume (<5%) of prostate.

Treatment plans using 5-mm PTV margins resulted in sufficient dose delivered to the prostate for all 15 patients in the cohort. This suggests that when using real-time tracking with careful setup to <10° of initial rotation and a 3-mm action level, 5-mm PTV margins are sufficient to overcome any adverse effects of intrafraction organ rotation. Using our institutional definition of a dosimetrically "sufficient" treatment, 12 of 15 patients would have received sufficient dose to the prostate with 3-mm PTV margins. Using only the first 3, 5, and 10 fractions, adequacy or inadequacy of treatment was predicted for 39 of 45, 42 of 45, and 45 of 45 cases. The relatively high predictive accuracy (87%) using motion only during the first three fractions is surprising, but consistent with prior reports of motion heterogeneity between patients, although not necessarily between fractions for a given patient (10, 11, 13).

Our model applied rigid transformations to structures of interest within a static dose cloud. To gauge the impact of tissue density variation, we calculated prostate and rectum–prostate interface dose for a patient with a distended rectum, with air-equivalent density manually assigned to the entire rectum structure. Loss of lateral scatter resulted in decreased dose at the air–tissue interface, and reduced attenuation in air resulted in a slight increase to mean and maximum prostate dose. Review of isodose lines (Fig. 5) and full dosimetric parameters (see Results) revealed that although the effect was relatively subtle, a radical change in rectal composition can cause inadequate treatment delivery, when adequacy is defined by $D_{min,\ actual} \geq 98\%\ D_{min,\ planned}$. Although this example illustrates the potential dose effect of a radical change in rectal composition, this has not been observed in clinical practice. For recalculation of daily dose using megavoltage CT imaging, Kupelian *et al.* reported <2% variation in delivered compared with planned dose to 95% of the prostate (20).

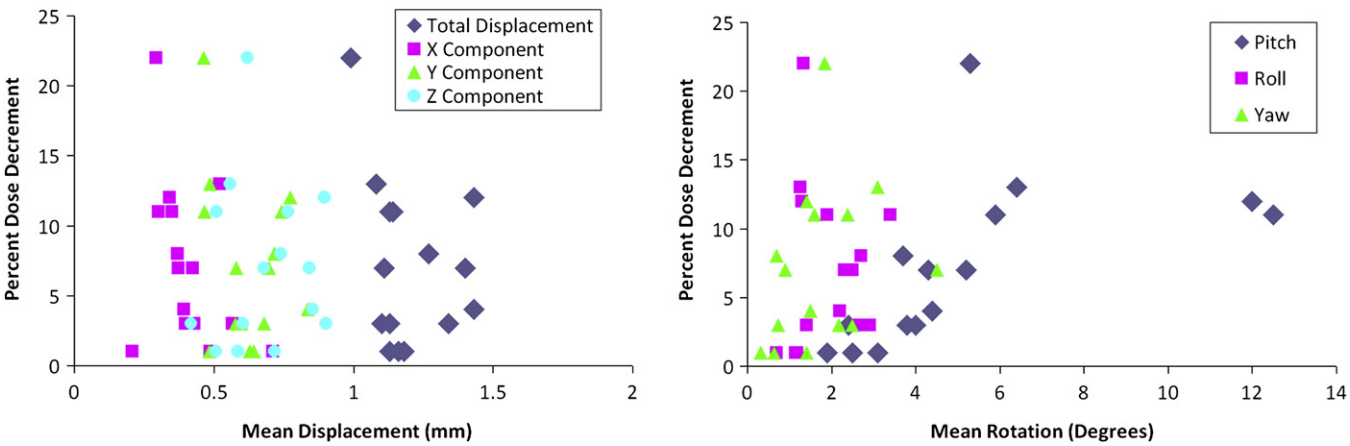

Fig. 7. (Left) Dose decrement as a function of mean isocenter displacement (left) along the x (left–right), y (superior–inferior), and z (anterior–posterior) axes, and composite displacement calculated using the distance formula. (Right) Dose decrement as a function of mean intrafraction pitch, roll, and yaw of the prostate for all patients based on 0-mm planning target volume (PTV) plans.

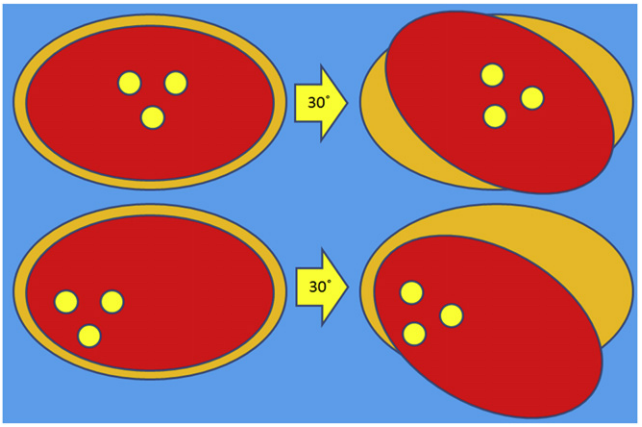

Fig. 8. Schematic illustration of the variable effect of transponder geometry as a gauge for rotation measurements. The fiducial markers are depicted by yellow circles, within the prostate (red) and planning target volume (PTV; orange). Rotations of 30° are shown about the centroid of the three beacons for idealized (top) and skewed (bottom) fiducial geometry. A rotation of a given magnitude (30° in this example) will carry different implications, depending on the reference axis of rotation.

We used intertransponder distance variability to evaluate the rigid body approximation, and found that deformation greater than 0.5 and 1.5 mm occurred less than 16% and 1% of the total treatment time, respectively. Our data support observations from a recent CT-based imaging study suggesting that the prostate may be treated as a rigid body (21). An MRI-based deformation study by Nichol *et al.* (22) revealed random interfraction deformation uncertainty of 1.5 mm, and average reduction in prostate volume of 0.5% per fraction during radiotherapy. Given the uncertainties of 0.8 mm and 0.4 mm with regard to the position of serial prostate contours and fiducial centroid localization, the data supports minimal impact of prostate deformation in the presence of physiologic rectal filling. Although reductions in prostate volume during radiotherapy were not accounted for in our model, a reduced prostate volume could potentially improve target coverage, as a reduction in target size effectively increases the PTV margin. The integration of real-time volumetric imaging during radiation therapy delivery would definitively answer questions about deformation and volume change, but were beyond the scope of the current study. Several groups are currently working toward development of magnetic resonance–guided radiotherapy that would potentially solve this problem by real-time dose recalculation (23–25).

Of note, our analysis applies only to treatment of the prostate while supine, and not treatment of the seminal vesicles or regional lymph nodes. Also, application of this technique to proton radiation therapy may be limited, as changes in tissue homogeneity can have significant dosimetric consequences.

CONCLUSION

We have provided a description of intrafraction translational and rotational motion of the prostate and a method to evaluate the sufficiency of individualized patient margins using real-time tracking. Our "automated" adaptive process does not require additional segmentation or image analysis workload for the physician, and is ready for implementation in the clinic.

REFERENCES

1. Beckendorf V, Guerif S, Prise EL, *et al*. 70 Gy versus (vs) 80 Gy dose escalation Getug 06 French Trial for Localized Prostate Cancer: Mature results. *Int J Radiat Oncol Biol Phys* 2008; 72:S96–S97.
2. Dearnaley DP, Sydes MR, Graham JD, *et al*. Escalated-dose versus standard-dose conformal radiotherapy in prostate cancer: First results from the MRC RT01 randomised controlled trial [see Comment]. *Lancet Oncol* 2007;8:475–487.
3. Kuban DA, Tucker SL, Dong L, *et al*. Long-term results of the M. D. Anderson randomized dose-escalation trial for prostate cancer [see Comment]. *Int J Radiat Oncol Biol Phys* 2008; 70:67–74.
4. Peeters ST, Heemsbergen WD, Koper PC, *et al*. Dose-response in radiotherapy for localized prostate cancer: Results of the Dutch multicenter randomized phase III trial comparing 68 Gy of radiotherapy with 78 Gy [see Comment]. *J Clin Oncol* 2006;24:1990–1996.
5. Zietman AL, DeSilvio ML, Slater JD, *et al*. Comparison of conventional-dose vs high-dose conformal radiation therapy in clinically localized adenocarcinoma of the prostate: A randomized controlled trial [see Comment] [Erratum appears in *JAMA* 2008;299:899–900]. *JAMA* 2005;294:1233–1239.
6. Aubry JF, Beaulieu L, Girouard LM, *et al*. Measurements of intrafraction motion and interfraction and intrafraction rotation of prostate by three-dimensional analysis of daily portal imaging with radiopaque markers. *Int J Radiat Oncol Biol Phys* 2004;60:30–39.
7. Chen J, Lee RJ, Handrahan D, *et al*. Intensity-modulated radiotherapy using implanted fiducial markers with daily portal imaging: Assessment of prostate organ motion. *Int J Radiat Oncol Biol Phys* 2007;68:912–919.
8. Britton KR, Takai Y, Mitsuya M, *et al*. Evaluation of inter- and intrafraction organ motion during intensity modulated radiation therapy (IMRT) for localized prostate cancer measured by a newly developed on-board image-guided system. *Radiat Med* 2005;23:14–24.
9. Kotte AN, Hofman P, Lagendijk JJ, *et al*. Intrafraction motion of the prostate during external-beam radiation therapy: Analysis of 427 patients with implanted fiducial markers. *Int J Radiat Oncol Biol Phys* 2007;69:419–425.
10. Kupelian P, Willoughby T, Mahadevan A, *et al*. Multi-institutional clinical experience with the Calypso System in localization and continuous, real-time monitoring of the prostate gland during external radiotherapy. *Int J Radiat Oncol Biol Phys* 2007;67:1088–1098.
11. Willoughby TR, Kupelian PA, Pouliot J, *et al*. Target localization and real-time tracking using the Calypso 4D localization system in patients with localized prostate cancer. *Int J Radiat Oncol Biol Phys* 2006;65:528–534.
12. Kuban D, Pollack A, Huang E, *et al*. Hazards of dose escalation in prostate cancer radiotherapy. *Int J Radiat Oncol Biol Phys* 2003;57:1260–1268.
13. Nederveen AJ, van der Heide UA, Dehnad H, *et al*. Measurements and clinical consequences of prostate motion during

a radiotherapy fraction. *Int J Radiat Oncol Biol Phys* 2002;53: 206–214.
14. D'Amico AV, Whittington R, Malkowicz SB, *et al*. Pretreatment nomogram for prostate-specific antigen recurrence after radical prostatectomy or external-beam radiation therapy for clinically localized prostate cancer. *J Clin Oncol* 1999;17: 168–172.
15. Olsen JR, Parikh PJ. Calypso real-time localization and tracking for treatment of prostate cancer with external beam radiotherapy. In: Image Guided Radiation Therapy. 1st ed. New York: McGraw-Hill; 2011. pp. 407–410.
16. Noel CE, Santanam L, Olsen JR, *et al*. An automated method for adaptive radiotherapy for prostate cancer patients using continuous fiducial based tracking. *Phys Med Biol* 2010;55:18.
17. Santanam L, Malinowski K, Hubenshmidt J, *et al*. Fiducial-based translational localization accuracy of electromagnetic tracking system and on-board kilovoltage imaging system. *Int J Radiat Oncol Biol Phys* 2008;70: 892–899.
18. Li HS, Chetty IJ, Enke CA, *et al*. Dosimetric consequences of intrafraction prostate motion. *Int J Radiat Oncol Biol Phys* 2008;71:801–812.
19. Cranmer-Sargison G. A treatment planning investigation into the dosimetric effects of systematic prostate patient rotational set-up errors. *Med Dosim* 2008;33:199–205.
20. Kupelian PA, Langen KM, Zeidan OA, *et al*. Daily variations in delivered doses in patients treated with radiotherapy for localized prostate cancer. *Int J Radiat Oncol Biol Phys* 2006;66:876–882.
21. Deurloo KE, Steenbakkers RJ, Zijp LJ, *et al*. Quantification of shape variation of prostate and seminal vesicles during external beam radiotherapy [Erratum appears in *Int J Radiat Oncol Biol Phys* 2005;61:1609]. *Int J Radiat Oncol Biol Phys* 2005;61: 228–238.
22. Nichol AM, Brock KK, Lockwood GA, *et al*. A magnetic resonance imaging study of prostate deformation relative to implanted gold fiducial markers. *Int J Radiat Oncol Biol Phys* 2007;67:48–56.
23. Raaymakers BW, Lagendijk JJ, Overweg J, *et al*. Integrating a 1.5 T MRI scanner with a 6 MV accelerator: Proof of concept. *Phys Med Biol* 2009;54:N229–N237.
24. Kirkby C, Stanescu T, Rathee S, *et al*. Patient dosimetry for hybrid MRI-radiotherapy systems. *Med Phys* 2008;35:1019–1027.
25. Dempsey J, Dionne B, Fitzsimmons J, *et al*. A real-time MRI guided external beam radiotherapy delivery system. *Med Phys* 2006;33:2254.